THE UA2 CENTRAL CALORIMETER

UA2 Collaboration (Bern-CERN-Copenhagen-Orsay-Pavia-Saclay)
Presented by A. Clark
CERN, Geneva, Switzerland

Summary

The UA2 experiment[1] was recently installed at the CERN Super Proton Synchrotron (SPS) proton-antiproton collider[2], to study collisions at an energy $\sqrt{s} = 540$ GeV.

A major objective of this experiment is to identify the weak intermediate bosons (Z^0,$W^{\pm}$) via their electronic decay modes:

$$\bar{p}p \to Z^0 + X^0 \; ; \quad Z^0 \to e^+e^-$$

$$\bar{p}p \to W^{\pm} + X^{\mp} \; ; \quad W^{\pm} \to e^{\pm}\nu \; .$$

Current theoretical models[3] predict a production cross-section $\sim 3 \times 10^{-33}$ cm^2 and a leptonic fraction $\sim 3\%$ for Z^0, $\sim 8\%$ for $W^{\pm}$.

The low expected Z^0, $W^{\pm}$ production rate implies the need for good electron identification and energy measurement over a maximal solid angle. The UA2 detector is instrumented over $\sim 80\%$ of the solid angle by segmented lead/scintillator sandwich counters, providing a $Z^0 \to e^+e^-$ acceptance of $\sim 63\%$. At luminosities $L \sim 10^{30}$ cm^{-2} s^{-1}, ~ 0.15 events/h should be detected with a mass resolution at the Z^0 peak $\sim 1.5\%$.

Another major objective of this experiment is to study high-p_T hadron jets. For this reason, and to enhance electron identification, segmented iron/scintillator sandwich counters are installed in the central region.

This talk describes the electromagnetic and hadronic calorimetry in the central region of the UA2 detector.

Experimental Apparatus

General

Figure 1 is a plan view of the apparatus. At the centre is the vertex detector. It consists of four multiwire proportional chambers (MWPC) with cathode strip readout, a cylindrical scintillator hodoscope, and two JADE-type drift chambers[4] with charge division and multi-hit readout. The detector is surrounded by 1.5 radiation lengths tungsten and a fifth proportional chamber (PROP5) to provide an accurate position measurement of e.m. showers. This chamber allows improved hadron rejection, and rejection against overlap background (a low-momentum hadron near a π^0, simulating an electron) in the following calorimeter.

Covering ± 1 rapidity units about 0, the vertex detector is surrounded by electromagnetic and hadron calorimeters.

The forward and backward directions (20° to 37.5°, 142.5° to 160°) are each instrumented by twelve toroidal-magnet sectors (0.38 T·m) and associated spectrometry. Following each sector, nine drift chamber planes allow a momentum measurement on charged tracks. After this, a 6 mm lead converter and two proportional-tube planes define the position of e.m. showers in a calorimeter.

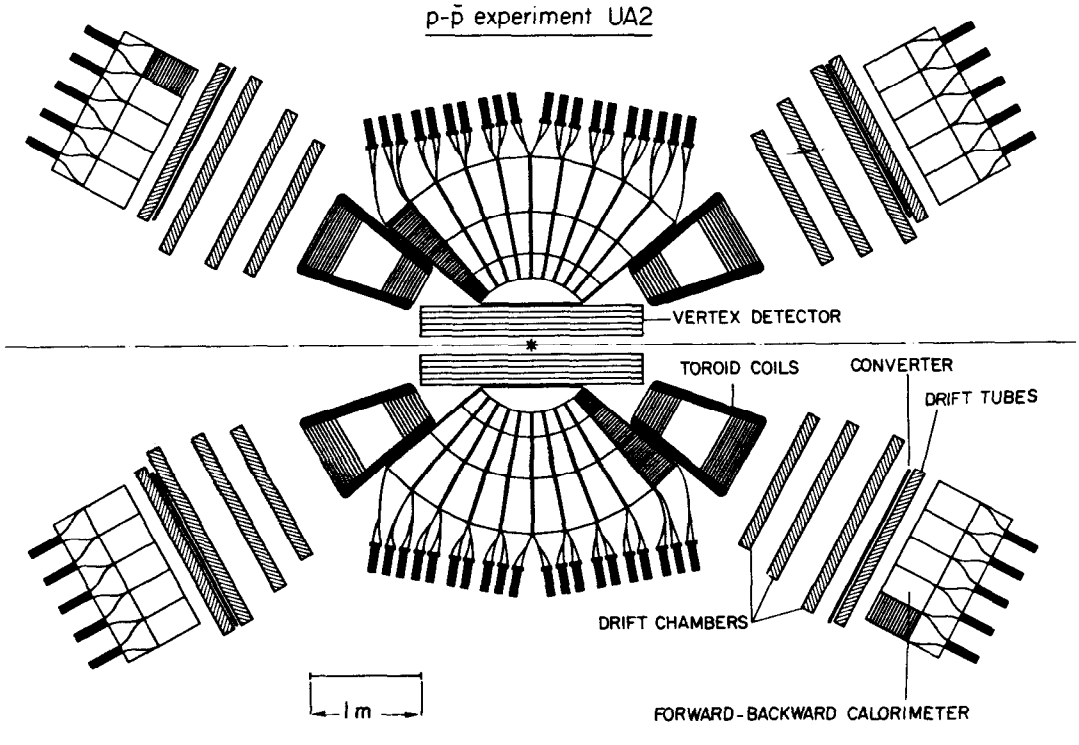

Fig. 1. Plan view of the UA2 detector.

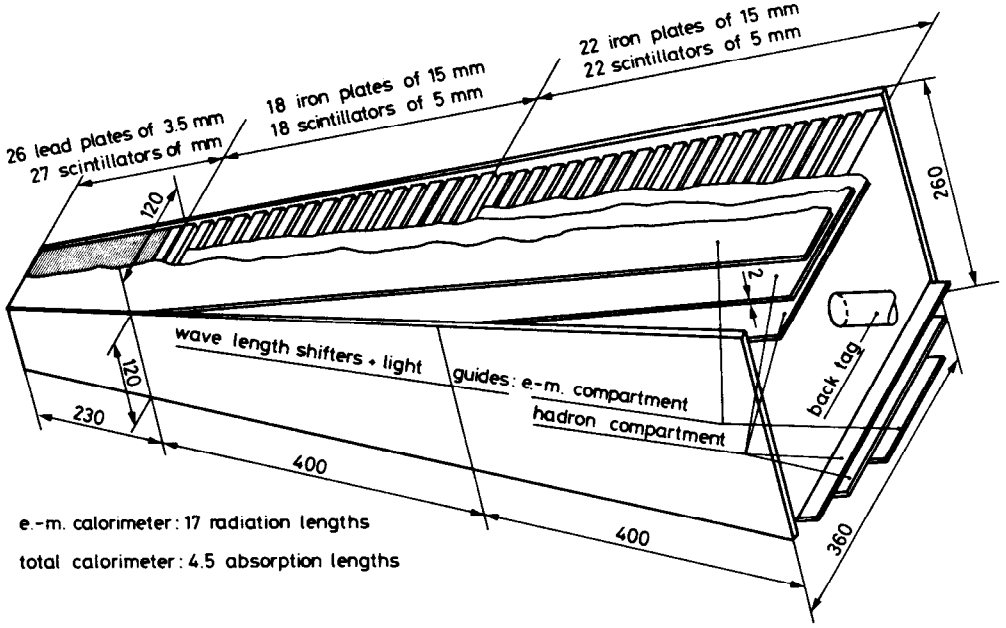

Fig. 2. Typical cell of the UA2 central calorimeter.

The 12 forward and 12 backward calorimeter sectors are each divided into ten cells (15° in ϕ, 3.5° in θ). Each cell is a lead/scintillator sandwich in two longitudinal sections (24 r.l. and 6 r.l.). The light of each section is collected in two phototubes via BBQ-doped wavelength-shifting light-guides. The calorimeter performance is similar to that of the central region.

Central Calorimeter

The lead/scintillator electromagnetic and iron/scintillator hadronic counters cover from 40° to 140° in polar angle, and all azimuthal angles. A spherical structure, the calorimeter is segmented into 240 individual cells (towers) pointing to the $\bar{p}p$ interaction vertex. Each cell has three longitudinal sections (plus PROP5). In addition, the last 0.35 attenuation lengths are separately measured to provide a tag on late hadronic showers. Each cell has an e.m. length $\sim$ 17.5 r.l. and a hadronic length $\sim$ 4 a.l. (Fig. 2).

The light of each section is transferred via 2 mm thick BBQ-doped light-guides to a total of seven phototubes per cell (XP2008, XP2012). The scintillator is 4 mm NE104B (e.m.), and 5 mm PMMA doped with 1% PBD, 0.1% POPOP, and 10% naphthalene (hadron). Wavelength-shifting techniques[5] minimize the dead-space between adjacent cells (Table 1). In practice the polar dead-space is negligible except for particles of normal incidence.

Table 1. Maximum separation between calorimeter cells

Compartment	Polar (mm)	Azimuth (mm)
EM	4.6 (light guide)	1 (Fe) + 1 mm (air)
HADRON 1	9 (light guide)	10 (Fe)
HADRON 2	13.6 (light guide)	10 (Fe)

To monitor phototube stability, a xenon light-flasher is associated with each azimuthal slice of ten cells. Light (diffused and filtered to approximate the light spectrum reaching the phototube) is passed via plastic fibres to the light-guide of each phototube. The net flasher stability and pulse-to-pulse variations in light output are monitored by a box containing three vacuum photodiodes. The relative stability of different azimuthal slices is monitored by sending light from each flash-tube to a box (J-BOX) containing a scintillator slab in front of three selected phototubes (XP2012). The stability of these phototubes is monitored by d.c. current measurements from ^{60}Co and ^{90}Sr sources.

An identical but independent flasher on each slice sends light to two scintillator plates of each e.m. compartment. The same photodiodes monitor flash stability.

Calibration Stability

An initial calibration of each cell was made using 10 GeV/c electrons (e.m. compartment) and 10 GeV/c muons (hadronic compartments). Since installation in November 1981, phototube gains have been monitored using the flash-tube of each slice, normalized with respect to the response of:

i) vacuum photodiodes (discarded because of gain changes);

ii) mean e.m. phototube response: the r.m.s. spread, for individual e.m. phototubes with respect to the mean, is ±2.6%; the mean hadron response is unchanged with respect to the e.m. phototubes, with an r.m.s. spread for individual tubes of 3%;

iii) J-BOX response: this indicates a mean change in e.m. light response of 0.5%, with an r.m.s. spread of 2%.

A mean change of $\leq$ 1% (r.m.s. of $\sim$ 0.6%) has been measured in e.m. response, from periodic ^{60}Co d.c. current measurements on each cell. In the extreme forward (proton) direction, the mean change reaches 1.7%, suggesting minor radiation damage.

The stability of the phototubes, between their initial calibration and installation at the $\bar{p}p$ collider, is being analysed.

Electron Response Measurements

In addition to the calibration of each e.m. cell with 10 GeV/c electrons, data were collected between 1 and 70 GeV/c for all 5 e.m. cell types. Figure 3 illustrates the nomenclature of this section.

Response Linearity and Resolution

Figure 4 shows the normalized light response to electrons of between 1 GeV/c and 70 GeV/c passing through the centre of an e.m. cell. Following a non-linearity correction $0.977\,[1.0 + 0.01\ \ln(E+1)]$, the light response can be estimated to $\lesssim \pm 1\%$. Figure 5 shows the variation of $\sigma/\sqrt{E}$ (0.14) with electron momentum. The beam momentum spread ($\sim 1\%$) has not been subtracted. In each figure, error bars represent the r.m.s. spread of *all* measurements on *all* cell types.

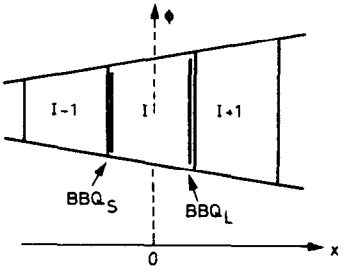

Fig. 3. Nomenclature used in following section. ϕ and x are measured with respect to the centre of the cell I.
BBQ_S = light response of small BBQ
BBQ_L = light response of large BBQ
$BBQ_{SL} = \sqrt{BBQ_S \cdot BBQ_L}$

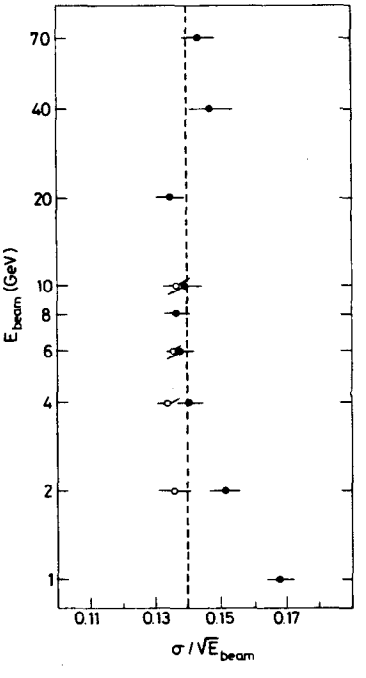

Fig. 4. Deviation from linearity of the light response BBQ_{SL} as a function of incident electron energy. The superimposed curve is $\propto [1 + 0.01\ \ln(E+1)]$.

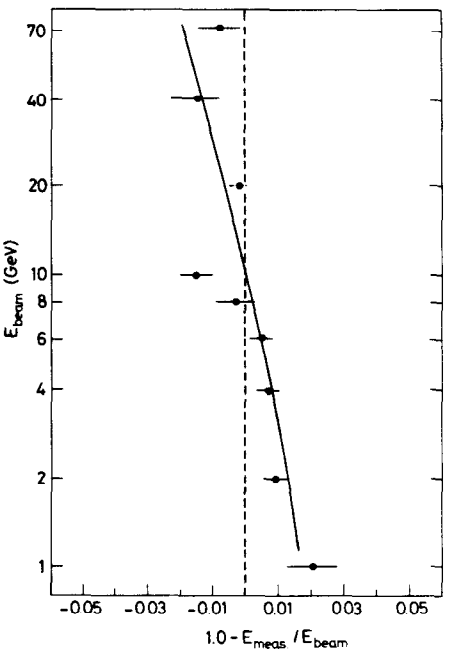

Fig. 5. Resolution of light response BBQ_{SL}, as a function of incident electron energy. (●) show data collected with tungsten converter 90 cm from the e.m. calorimeter. (○) show data collected with tungsten converter in final UA2 position.

Response Variation with Position (Normal Incidence)

Spatial scans were made for several examples of each cell type. The r.m.s. spread of measurements in different examples of the same cell type is < ±1%. Figure 6 shows the uncorrected response for cell 2 (the second smallest) as a function of position. Similar variations exist in other cell types. Figure 7 shows the same data after correction according as:

$$BBQ(corr) = BBQ(raw) \cdot \exp(corr)$$

$$corr = (A1.x + A2.x^2 + A3.x^3) + (B1 + B2.x + B3.x^2)|\phi| + (C1 + C2.x + C3.x^2)|\phi|^2 .$$

Constants A_i, B_i, C_i have been determined for each BBQ of the five cell types. Data from muons provide a consistent parametrization. For beam impacts > 5 mm from a cell interface, the r.m.s. spread of corrected light response for individual measurements of a cell type is < 1.1%. The resolution $\sigma/\sqrt{E}$ is unaffected. The ratio $BBQ_R = BBQ_S/BBQ_L$ provides a measure of the beam impact position in the cell ($\sigma \lesssim 5$ mm). However, because of differing light collection efficiencies for BBQ_S and BBQ_L, a variation of light response exists along each BBQ_R contour. For that small class of e.m. showers having no associated track or PROP5 signal, this variation defines the effective resolution of the e.m. calorimeter.

Response Near a Cell Interface (Normal Incidence)

The azimuthal separation between two cells is small, and a maximum response correction of 10% is required within ±2 mm of the cell interface. Few normal-incidence electrons pass through the BBQ (smeared $\bar{p}p$ vertex). At the BBQ interface, $\sim 20\%$ of electrons are within 3 st. dev. of the peak, and $\sigma/E \simeq 0.25/\sqrt{E}$. The light response of remaining events is distributed *below* the peak (longitudinal escape and Čerenkov light).

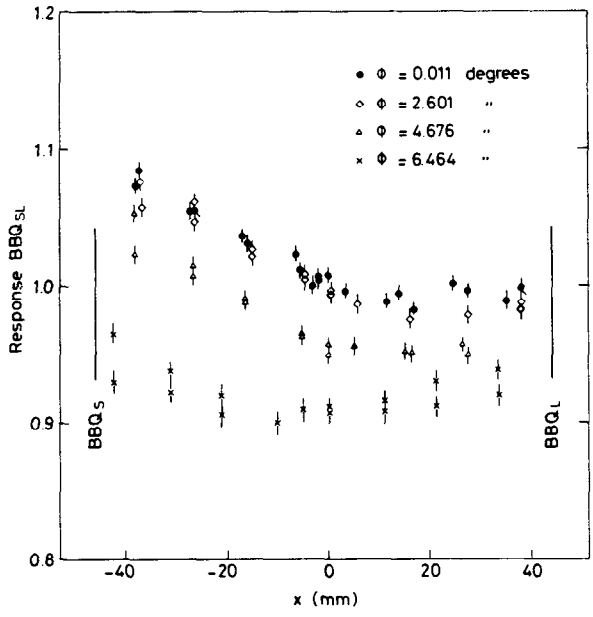

Fig. 6. Variation of light response BBQ$_{SL}$ with position, in cell type 2 of the e.m. calorimeter.

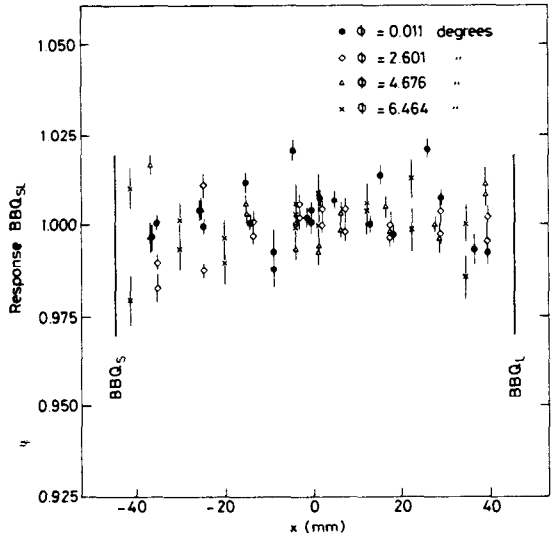

Fig. 7. Data of Fig. 6, after correction for the position of beam impact in calorimeter.

The UA2 calorimeter is short (4 a.l.), so significant longitudinal escape is expected. However, high-energy hadron jets should be better contained since their behaviour is similar to that of a single particle interacting at the calorimeter entrance. Data exist both for single particles and for simulated jets.

Event Selection

To ensure good energy containment, cuts were applied: E(hadron section 2)/E(calorimeter) $\leq$ 0.8, and E(e.m.) $\geq$ 1 GeV or E(hadron section 1) $\geq$ 1.5 GeV. The resultant event efficiency is shown in Fig. 8.

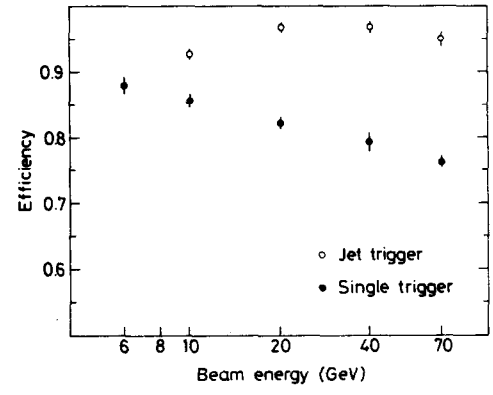

Fig. 8. Efficiency of detection in hadron calorimeter as a function of incident π^- energy. Applied cuts are described in text.

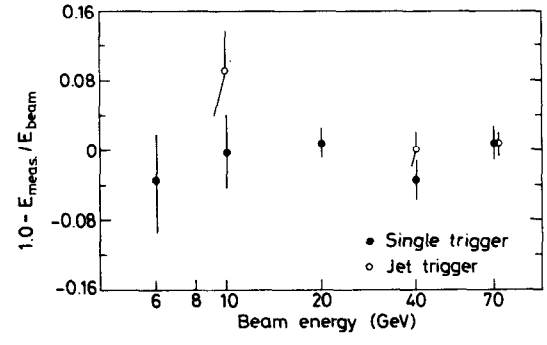

Fig. 9. Deviation from linearity of the light response BBQ$_{SL}$ as a function of incident π^- energy.

Non-Normal Beam Impact

At the $p\bar{p}$ collider, the interaction vertex is smeared along the beam direction with $\sigma \sim 10$ cm, and data were collected to simulate vertices in the range $-20 < z < 20$ cm. For $|z| > 2$ cm, no deterioration of the efficiency or resolution is measured near the BBQ interface, and no additional response corrections are required. Using the correction formulae above, the average response at each vertex position changes by < 1.4% with respect to normal incidence. The r.m.s. spread of individual measurements is < ±1% for each cell type.

Hadron Response Measurements

Data have been collected at π^- momenta of 1 to 70 GeV/c and π^+ momenta of 1 and 2 GeV/c. Preliminary results are shown for π^- data of momenta above 6 GeV/c.

Light Response

A fit was made to normal-incidence JET and SINGLE data to find parameters, relating the response of each compartment, that optimize the response linearity (Fig. 9). The resultant resolution is shown in Fig. 10.

Response Uniformity

The above light-response analysis used available data in the median plane of each cell ($\phi \simeq 0$), with linear attenuation corrections. The resultant response was uniform to < ±4% for each cell type. For normal-incidence data near a BBQ interface, the acceptance is reduced for SINGLE triggers, but not for JET triggers (Fig. 11). The resolution is not significantly affected, as shown in Fig. 12.

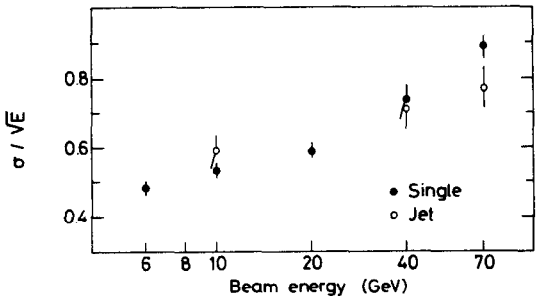

Fig. 10. Resolution of light response BBQ_{SL} as a function of incident π^- energy.

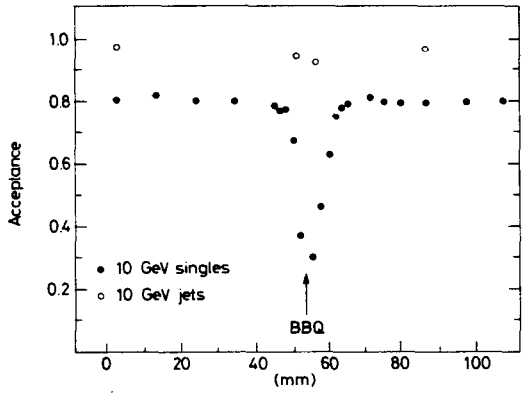

Fig. 11. Variation of π^- acceptance across cell interface of the central calorimeter.

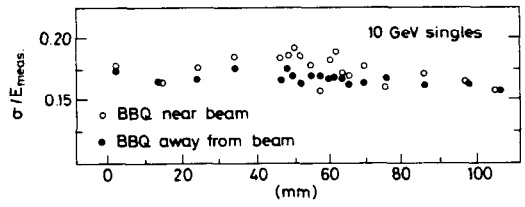

Fig. 12. Variation of π^- resolution across cell interface of central calorimeter.

Non-Normal Incidence

Data collected at an effective vertex position of ±10.4 cm shows an average change in light response of < ±1%. The resolution is unchanged. The variation in aperture across a BBQ interface is reduced to < ±5% for SINGLE triggers.

References

1. UA2 Collaboration (M. Banner et al.), CERN/SPS/78-08 (1978) and CERN/SPS/78-54 (1978).
2. C. Rubbia, P. McIntyre and D. Cline, in Proc. Int. Neutrino Conference, Aachen, 1976 (eds. H. Faissner, H. Reithler and P. Zerwas) (Vieweg, Braunschweig, 1977), p. 683.
   S. Van der Meer, CERN/SPS/423 (1978).
   Design study of a $p\bar{p}$ colliding beam facility, CERN/PS/AA 78-3 (1978).
3. See, for example: C. Quigg, Rev. Mod. Phys. 44, 297 (1977).
4. JADE Collaboration (W. Farr et al.), Nucl. Instrum. Methods 156, 283 (1977).
5. R.L. Garwin, Rev. Sci. Instrum. 31, 1010 (1960).
   W.B. Atwood, C.Y. Prescott, L.S. Rochester and B.C. Barish, SLAC-TM-76-7 (1976).